Contributions of principal neocortical neurons to magnetoencephalography and electroencephalography signals

Shingo Murakami and Yoshio Okada

Department of Neurology and Biomedical Research and Integrative Neuro-Imaging (BRaIN Imaging) Center, University of New Mexico School of Medicine, Albuquerque, NM 87131, USA

A realistically shaped three-dimensional single-neuron model was constructed for each of four principal cell types in the neocortex in order to infer their contributions to magnetoencephalography (MEG) and electroencephalography (EEG) signals. For each cell, the soma was stimulated and the resulting intracellular current was used to compute the current dipole *Q* for the whole cell or separately for the apical and basal dendrites. The magnitude of *Q* is proportional to the magnetic field and electrical potential far from the neuron. A train of spikes and depolarization shift in an intracellular burst discharge were seen as spikes and an envelope in *Q* for the layer V and layer II/III pyramidal cells. The stellate cells lacked the envelope. As expected, the pyramidal cells produced a stronger *Q* than the stellate cells. The spikes produced by the layer V pyramidal cells ($n = 4$) varied between −0.78 and 2.97 pA m with the majority of the cells showing a current toward the pia (defined as positive). The basal dendrites, however, produced considerable spike currents. The magnitude and direction of dipole moment are in agreement with the distribution of the dendrites. The spikes in *Q* for the layer V pyramidal cells were produced by the transient sodium conductance and potassium conductance of delayed rectifier type; the conductances distributed along the dendrites were capable of generating spike propagation, which was seen in *Q* as the tail of a triphasic wave lasting several milliseconds. The envelope was similar in magnitude (−0.41 to −0.90 pA m) across the four layer V pyramidal cells. The spike and envelope for the layer II/III pyramidal cell were 0.47 and −0.29 pA m, respectively; these values agreed well with empirical and theoretical estimates for guinea pig CA3 pyramidal cells. Spikes were stronger for the layer IV spiny stellate (0.27 pA m) than the layer III aspiny stellate cell (0.06 pA m) along their best orientations. The spikes may thus be stronger than has been previously thought. The *Q* for a population of stellate cells may be weaker than a linear sum of their individual *Q* values due to their variable dendritic geometry. The burst discharge by pyramidal cells may be detectable with MEG and EEG when 10 000–50 000 cells are synchronously active.

(Resubmitted 14 January 2006; accepted after revision 6 April 2006; first published online 13 April 2006)
Corresponding author S. Murakami: Division of Molecular and Cellular Pharmacology, Department of Pharmacology, Graduate School of Medicine, Osaka University, 2-2 Yamada-oka, Suita, Osaka 565-0871 Japan.
Email: murakami@pharma2.med.osaka-u.ac.jp

Magnetoencephalography (MEG) and electroencephalography (EEG) are at present the only non-invasive techniques capable of measuring electrical activity from the brain with a millisecond time resolution. Although magnetic resonance imaging (MRI) and positron emission tomography (PET) are quite useful, they measure biochemical activity with low time resolution. These differences make MEG and EEG useful for studying human brain functions. They are used to infer the location of each active tissue in the brain and the time course of activity in each area. However, it is still generally difficult to interpret MEG and EEG in terms of the underlying physiological events at the cellular level, in part due to a lack of understanding of the relationship between cellular events and population signals.

In the past 20 years our understanding of CNS electrophysiology has changed dramatically with the discovery of voltage-sensitive channels in neurons (Llinás, 1988; Johnston *et al.* 1996; Hille, 2001; Migliore & Shepherd, 2002). It is now well established that neurons have a variety of voltage-dependent ion-gated intrinsic conductances. These discoveries have necessitated an examination of the

© 2006 The Authors. Journal compilation © 2006 The Physiological Society DOI: 10.1113/jphysiol.2006.105379

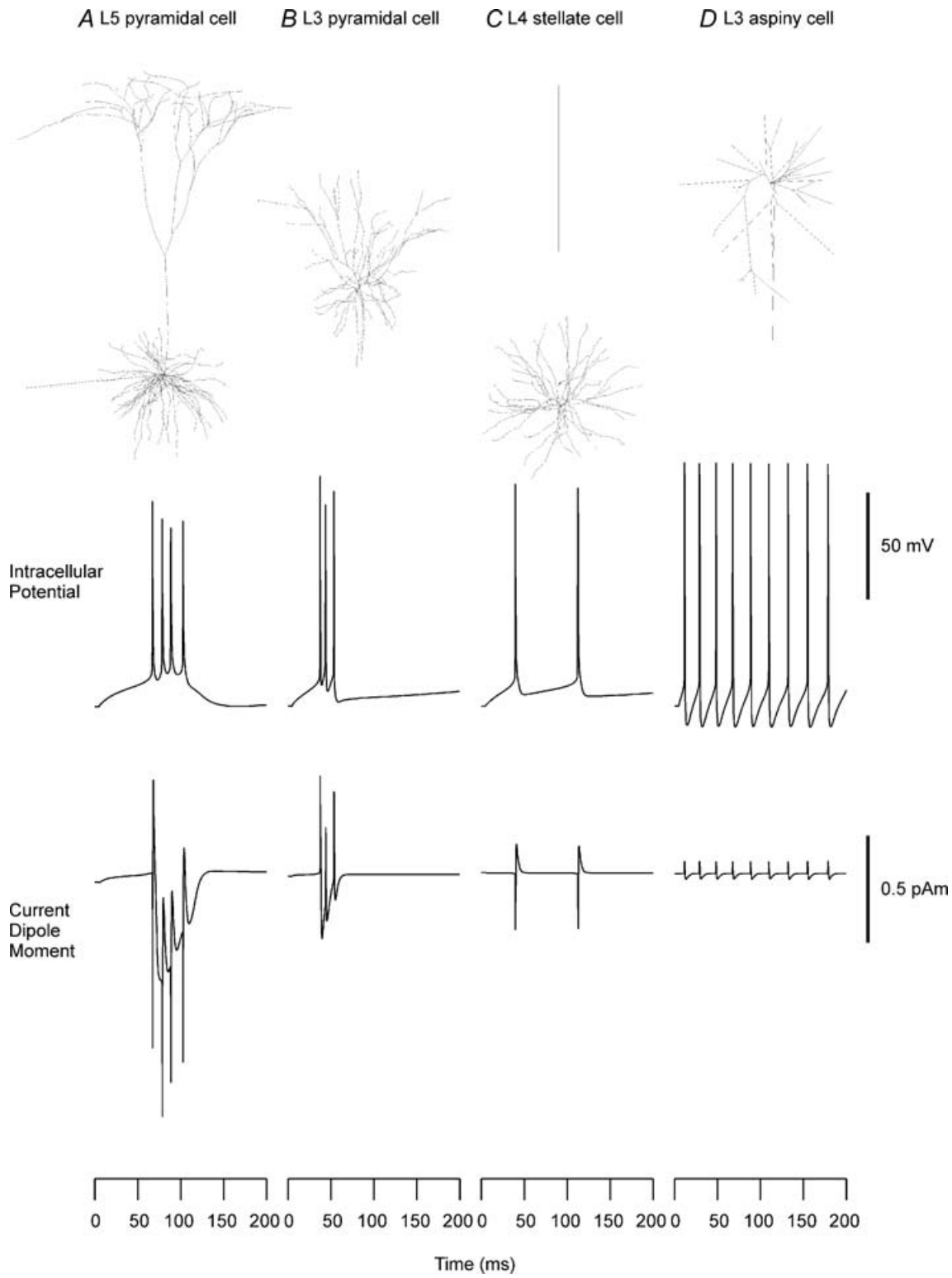

Figure 1. Reconstructed shapes, firing patterns and intracellular current dipole moments of neocortical neurons

Reconstructed neuron models from cat visual cortex (*A–C*) and rat somatosensory cortex (*D*); shapes of cells (row 1), evoked firing patterns (row 2) and current dipole moments (row 3) for a layer V pyramidal cell (*A*), layer II/III pyramidal cell (*B*), layer IV spiny stellate cell (*C*), and layer III aspiny cell (*D*). Geometries of the cells were taken from the 1996 Mainen model. A constant current was injected into the soma (200 pA, 100 pA, 70 pA, 50 pA for *A–D*, respectively). Positive polarity indicates currents directed from a deep layer to the surface for the pyramidal

© 2006 The Authors. Journal compilation © 2006 The Physiological Society

genesis of MEG and EEG signals in the neocortex in light of the modern concepts of CNS neurons.

Recently, it has been shown that both evoked MEG and EEG signals from the hippocampus can be understood within a single theoretical framework (Okada & Wu, 1998; Murakami *et al.* 2002, 2003). Murakami *et al.* (2002, 2003) revised the mathematical network model of Traub (Traub *et al.* 1991, 1992, 1993) for the CA3, which has been thoroughly validated for intracellular data by Traub and colleagues (Traub & Miles, 1991; Traub *et al.* 1991, 1994, 1999). They have observed the importance of dendritic branching and diameter in explaining MEG and EEG signals, and have revealed the need for models in which neurons have realistic shapes for analysing the genesis of MEG and EEG signals (Murakami *et al.* 2002). The modified model was able to provide a quantitatively accurate account of evoked magnetic fields from the CA3 slice, extracellular field potentials within the slice as well as intracellular potentials from the pyramidal cells. These findings have suggested that realistic dendritic anatomy needs to be taken into account to infer the origin of MEG and EEG signals arising from the neocortex where the cell geometry is diverse.

In the present analysis, a realistically shaped multicompartment model was developed for each principal neuron in the neocortex to elucidate their contributions to MEG and EEG signals. MEG and EEG signals due to individual neurons at large distances are proportional to the magnitude of the net intracellular current dipole, $\boldsymbol{Q}$, in each cell (Barr *et al.* 1966; Geselowitz, 1967). Thus, mathematical models were used to compute the intracellular potentials, and the intracellular currents in separate compartments of the model cell were vectorially summed to compute $\boldsymbol{Q}$. Four layer V pyramidal cells, one layer II/III pyramidal cell, one spiny stellate cell in layer IV and one aspiny cell in layer III were selected for this study. We used $\boldsymbol{Q}$ to infer how various types of firing patterns in intracellular potential such as the spikes produced by sodium currents and depolarization shift during spike bursts appear in MEG and EEG signals. The analysis was carried out separately for the apical and basal dendrites and the whole cell.

In the classic literature, MEG and EEG signals have been thought to be due to intracellular currents in the pyramidal cells that are perpendicular to the cortical surface (Llinás & Nicholson, 1974; Okada, 1982). This explanation is based on the work of Lorente de Nó (1947) who developed the concept of 'open' and 'closed' field configurations. Cells with the dendrites along the predominant direction (i.e. the longitudinal axis) are said to have 'open-field' configurations because the electrical fields from such cells extend over long distances. These cells, typically pyramidal cells, may produce EEG signals that can be measured as far as the scalp. Cells with radially symmetric dendrites such as aspiny stellate cells are said to have closed-field configurations because their electrical fields are confined within the volume of the cells. These cells are not expected to produce EEG signals at large distances. Analogously, MEG signals are believed to be due to cells with open-field configurations (Okada, 1982). However, this concept of Lorente de Nó has been analysed only qualitatively in the context of the genesis of MEG and EEG from the neocortex. The present analysis quantitatively examined the contributions of principal neocortical neurons to MEG and EEG signals.

Methods

Mathematical model

The neocortical models used in this study are based on the 1996 Mainen model (Mainen & Sejnowski, 1996) and morphological data from the 1998 Stuart model (Stuart & Spruston, 1998). The Mainen model, written in NEURON, is available from a public website (http://senselab.med.yale.edu/senselab/modeldb/).

Figure 1 shows the four principal cells that are represented in the Mainen model. The pyramidal cells and the spiny stellate cell are from the cat visual cortex and the aspiny stellate cell is from the rat somatosensory cortex. Each cell is described by a three-dimensional multicompartment model in which each segment of the dendrites, axon and soma is represented by a cylinder with a maximum length of 50 μm. The dendritic membrane of spiny neurons is increased to account for spines (by adding 0.83 μm^2 per linear μm of dendrite). Each compartment has its own geometrical properties (e.g. length and diameter), passive properties (e.g. membrane capacitance, membrane resistance and intracellular resistance) and five voltage-dependent conductances: sodium conductance, g_{Na}; potassium conductance of delayed rectifier type, $g_{\mathrm{K(DR)}}$; slow non-inactivating potassium conductance of the M type, $g_{\mathrm{K(M)}}$; calcium conductance, g_{Ca}; and potassium conductance of the C type, $g_{\mathrm{K(C)}}$ (corresponding to I_{Na}, I_{Kv}, I_{Km}, I_{Ca} and I_{KCa} in Mainen & Sejnowski (1996), respectively).

Morphological data of three more layer V pyramidal cells from the rat somatosensory cortex (Stuart & Spruston, 1998) were also taken from the same NEURON website and the same channels from the Mainen 1996

cells. Unit dipoles that maximize the dot products were used for the layer IV spiny and the layer III aspiny cells. Positive polarity indicates currents directed from the bottom to the top of the figure for layer IV spiny stellate cell and layer III aspiny cell.

© 2006 The Authors. Journal compilation © 2006 The Physiological Society

model were incorporated into the cells. The channel distributions in the 1996 Mainen model were used in the simulation results shown in Figs 1, 2 and 3. The three conductances – $g_{K(M)}$, g_{Ca} and $g_{K(C)}$ – were removed in the simulation study reflected in Fig. 4 to evaluate the roles of g_{Na} and $g_{K(DR)}$, which shape the sodium spikes. The simulations for Fig. 4*A* were obtained with g_{Na} and $g_{K(DR)}$ in the soma, but with no g_{Na} and $g_{K(DR)}$ in the dendrites in order to calculate the shape of the sodium spike in a classic neuron model with completely passive dendrites. The simulations in Fig. 4*B* were obtained with a modified neuron model capable of exhibiting back-propagation in the dendrites. The g_{Na} and $g_{K(DR)}$ were uniformly distributed throughout the basal and proximal apical dendrites with the same channel densities as in the soma, in accordance with findings such as a constant density at the soma and proximal apical dendrite (Stuart & Sakmann, 1994), the existence of Na^+ spikes in the basal dendrites (Antic, 2003) and a constant density of $g_{K(DR)}$ at the soma and proximal apical dendrites (Bekkers, 2000; Korngreen & Sakmann, 2000). Figure 4C was obtained with g_{Na} and $g_{K(DR)}$ uniformly distributed throughout all of the dendrites, including the distal apical dendrites, with the same channel densities as in the soma, in accordance with findings of existence of g_{Na} in the distal apical dendrites and active propagation into the distal apical dendrites (Schiller et al. 1995; Larkum et al. 1999; Williams & Stuart, 2000). A conductance of 40 pS μm^{-2} from Stuart & Sakmann (1994) has been used as the *de facto* standard value of maximum g_{Na}, and is used for Fig. 4*A*–*C*. However, neocortical pyramidal cells demonstrate a large increase in g_{Na} during the development period (E16–P50) (Huguenard *et al.* 1988). The normalized maximum conductances are near 10 pS μm^{-2} in embryonic rats and increase 6- to 10-fold during the first two postnatal weeks. Therefore, 100 pS μm^{-2} was also used for g_{Na} throughout the basal and apical dendrites in Fig. 4*D* in order to check for possible parameter dependencies. The value of $g_{K(DR)}$ (5 pS μm^{-2}) was selected by trial and error so that sodium spikes could be reproduced. The anatomies and the channel densities in the axon and initial segment were the same as in the original Mainen model for all figures. The axon in all of our model calculations is abbreviated and the contribution of the axonal arbor is omitted in the present study due to lack of adequate anatomical data.

Calculation of the current dipole *Q* and its moment

Each cell was stimulated by intracellular injection of a constant current to the soma. The stimulation produced a depolarization in the soma, which in turn led to a cascade of activation of voltage-sensitive channels. The voltage gradient along the longitudinal axis of each compartment produced intracellular current. The intracellular current in each compartment k can be thought of as a current dipole $\boldsymbol{Q}_k$. It is a vector quantity defined as $\boldsymbol{Q}_k = IL\boldsymbol{dr}$, where I is the current along the longitudinal axis, L is the length of each compartment and $\boldsymbol{dr}$ is a unit direction vector for the compartment. I is related to longitudinal current density J and cross-sectional area A of each cylindrical compartment by $I = JA$. The magnitude of $\boldsymbol{Q}_k$ is called the current dipole moment and denoted by the scalar quantity Q. In the present study it is expressed in the unit of picoampere metre (pA m). The $\boldsymbol{Q}_k$ in each compartment k was calculated from the three-dimensional position and direction of each compartment. The net Q for the entire layer V pyramidal cell was calculated by computing the $\boldsymbol{Q}_k$ for each compartment, then forming the sum of the dot product of each current dipole and the unit vector orthogonal to the surface of the cortex. The vector $\boldsymbol{Q}$ is projected to the unit vector orthogonal to the surface of the cortex because processes of cortical neurons are arranged predominantly along this longitudinal axis. Positive polarity indicates currents directed from a deep layer to the surface. The net Q for the layer II/III pyramidal cell was calculated in the same way. For the spiny stellate cell, the orientation of the cell relative to the pial surface was chosen as the direction of the unit dipole that maximized the dot product with the net current dipole in all the dendritic compartments. The unit dipole that maximized the dot product was also used for the layer III aspiny stellate cell since its orientation relative to the pia was not known. Positive polarity indicates currents directed from the bottom to the top of the figure for the layer IV spiny stellate cell and the layer III aspiny cell. In some calculations, Q was calculated for a specific segment such as the apical or basal dendrites of the cell.

The contributions of principal neurons to MEG and EEG signals can be evaluated by examining properties of $\boldsymbol{Q}$ for these neurons. The magnetic field $\boldsymbol{B}$ and electrical potential Φ at the scalp can be expressed as a mixture of the intracellular currents, called primary currents, and the secondary currents at boundaries between spaces differing in electrical conductivity such the brain, skull and scalp (Barr *et al.* 1966; Geselowitz, 1967, 1970; Sarvas, 1987; Huang *et al.* 1990; Hämäläinen *et al.* 1993). The primary current equals the population $\boldsymbol{Q}$, which is a vector sum of $\boldsymbol{Q}$ values produced by an ensemble of neurons in each active region of the brain. The secondary currents depend on the primary current linearly and they can be computed from the population $\boldsymbol{Q}$ once the conductor geometry of the head is known. The magnetic field $\boldsymbol{B}$ is due to the component of $\boldsymbol{Q}$ tangential to the inner skull surface (Sarvas, 1987; Hämäläinen *et al.* 1993), whereas Φ on the scalp is due to both the tangential and radial components of $\boldsymbol{Q}$. Remembering that the $\boldsymbol{Q}$ is orientated perpendicular to the pial surface, one sees that the $\boldsymbol{B}$ is predominantly due to neuronal activity in sulci and Φ to activity in both sulci

© 2006 The Authors. Journal compilation © 2006 The Physiological Society

and gyri of the cerebral cortex. The temporal waveforms of MEG and EEG signals are proportional to the magnitude of the population $\boldsymbol{Q}$.

In the present study, the contribution of glial cells was not considered because they show limited changes in their membrane potential (Haydon, 2001). Moreover, they form a syncytium and thus it would be necessary to construct a network model to evaluate their contributions, which is beyond the scope of the present analysis.

Results

Amplitude and waveform of *Q* for the principal neocortical neurons

The intracellular potential in the soma and Q of the whole cell were calculated for each of four cell types with Mainen's original parameters (Fig. 1). Various intracellular firing patterns specific to the cell types were seen as in the study by Mainen & Sejnowski (1996). The pyramidal cells showed bursting behaviour, whereas the stellate cells showed tonic firing. The Qs for the pyramidal cells consisted of a train of spikes riding on an envelope resembling the depolarization shift in intracellular potential. In the layer V pyramidal cell, the sharp spike was directed initially downward, i.e. toward the basal dendrites, followed by a spike directed upward, i.e. toward the apical dendrites. The current of depolarization shift was directed downward. In the layer II/III pyramidal cell, the spike was upward, i.e. toward the pia, unlike the layer V cell, whereas the depolarizing burst current seen in Q was directed downward like the layer V cell. The Qs for both the spiny and aspiny stellate cells consisted of a train of biphasic spikes lacking the envelope, corresponding to their tonic firing patterns.

The relative strengths of Q were consistent with the classic notion of open and closed field configurations. The initial spikes were -0.78 and 0.47 pA m peak-to-baseline and the envelopes of Q were -0.46 and -0.29 pA m for the layer V pyramidal cell and layer II/III pyramidal cell, respectively. The spikes were 0.27 and 0.06 pA m, peak to baseline, for the layer IV spiny stellate cell and layer III aspiny stellate cell, respectively. In the case of the spiny stellate cell and the aspiny stellate cell, the direction of the cell relative to the pial surface was not known for the Mainen model. Thus, this direction was estimated from a vector that maximized the dot product with the $\boldsymbol{Q}$ in individual dendrites. Since the direction of net dipole may be variable, the net magnitude could be smaller for an ensemble of spiny and aspiny stellate cells. These results suggested that the layer V and II/III pyramidal cells are the major contributors to MEG and EEG signals.

The results for the layer V pyramidal cell model of Mainen showed a strong Q associated with the initial spike and the direction of the spike was stronger toward the basal dendrites than toward the apical dendrites. Since the strong contribution of the basal dendrites was counter-intuitive, additional simulation studies were carried out for the layer V pyramidal cell class by taking the anatomical data from Stuart & Spruston (1998), shown at the top in Fig. 2. As noted in Methods, the properties of these cell models were the same as the Mainen model except for their cellular geometries. The basal dendrites of these cells were less dense than the cell modelled by Mainen & Sejnowski (1996). As shown in the middle row, their intracellular bursting patterns differed from each other and from the Mainen model. The first pyramidal cell (Fig. 2*A*) showed a repetitive firing pattern with almost no bursting. The second cell (Fig. 2*B*) showed a clearer bursting pattern with a superimposed tonic firing. The third cell (Fig. 2*C*) exhibited a short-lasting bursting firing pattern like the Mainen model, but with some after-discharges.

Their Qs, shown at the bottom, contained some similarities and differences among each other. The spikes and depolarizing shift in intracellular potential were seen as initial spikes and as an envelope in Q just like the Mainen model. The absolute magnitude was of the same order for the spikes in the three cells (0.50–2.97 pA m, peak to baseline), but their directions were different from the Mainen model. The current during the initial spike was directed toward the basal dendrites in the original Mainen model, but it was directed toward the apical dendrites for the three cells taken from Stuart & Spruston (1998). In contrast to the spikes, the waveform and magnitude of the wave reflecting the depolarization shift were quite similar across the four cells (-0.41 to -0.90 pA m).

Contribution of the apical and basal dendrites to MEG and EEG

The contributions of the apical and basal dendrites of the four layer V pyramidal cells to MEG and EEG signals were determined separately by calculating the Q associated with the intracellular currents in these two regions of the cell (Fig. 3). Continuous curves are Qs produced by the apical or basal dendrites. Dotted curves are those produced by the whole cell, identical to those in Figs 1 and 2.

There are some interesting features that provide insights into the flow of currents when current is injected into the soma to activate the neuron. Firstly, the direction and shape of the spike in the apical dendrites are consistent across the four cells. They were all directed toward the pia with spike amplitudes between 0.78 and 2.37 pA m. Secondly, the initial spike current for the basal dendrites was directed toward a deep layer in most cells (Fig. 3*A*–*C*), but it was directed toward the pia in one cell (Fig. 3*D*). The magnitude was also variable, ranging between -1.68 and 0.63 pA m. Thirdly, the negative wave following the spike, which forms the overall envelope of Q, was dominated by the current in the apical dendrites during the intracellular burst.

© 2006 The Authors. Journal compilation © 2006 The Physiological Society

The anatomical basis for the variable spike direction and magnitude was investigated by examining the distribution of dendritic branches in the layer V pyramidal cells, separately for the apical and basal segments. A volume vector element was computed for each compartment of all the dendritic branches. Its direction was parallel to the longitudinal axis of the compartment and its moment was the product of the surface area and length of the compartment. The volume vector elements were then vectorially summed and projected to the unit vector perpendicular to the pia. The total vector indicates the predominant direction and total effective volume of

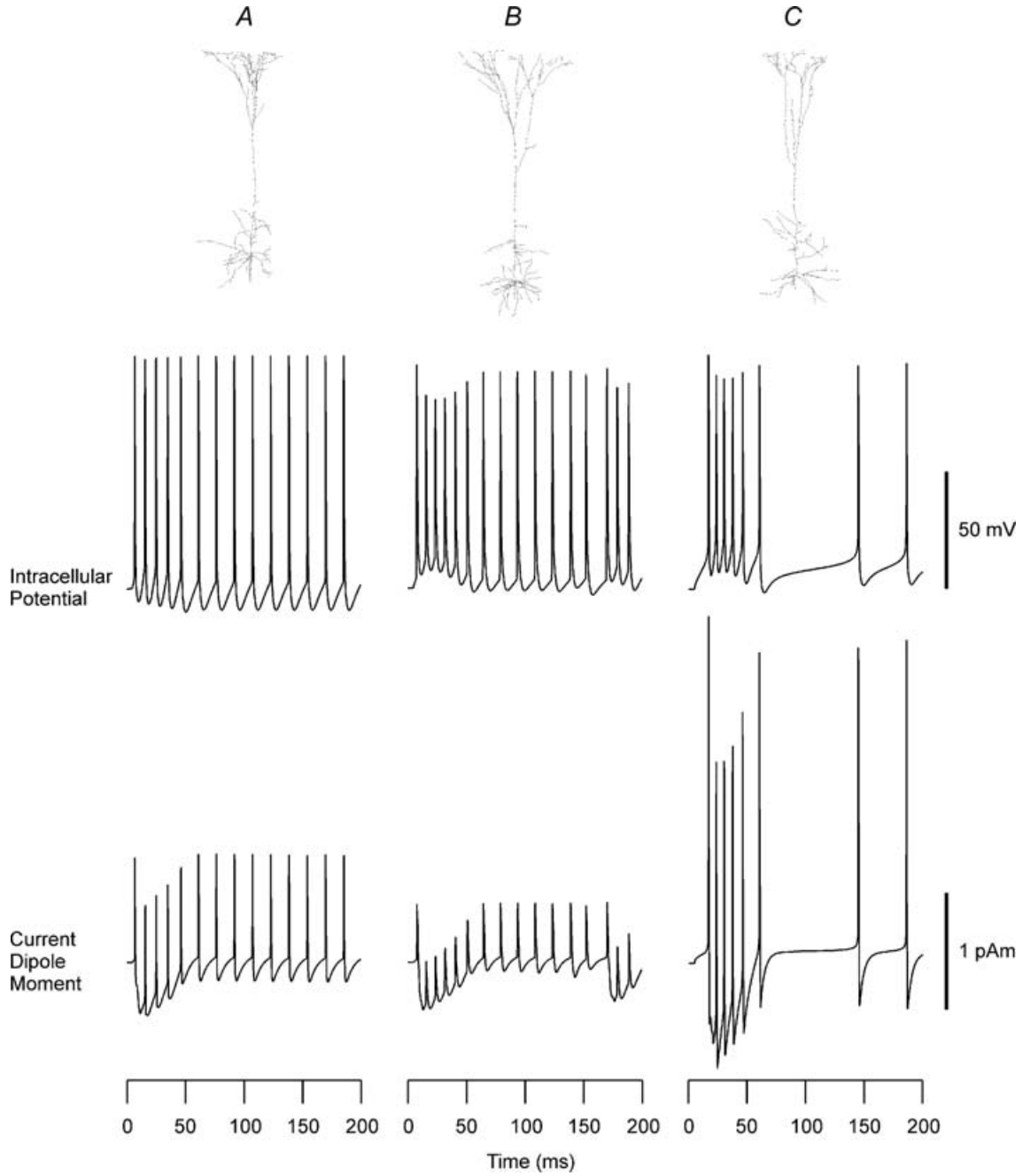

Figure 2. Reconstructed shapes, firing patterns and intracellular current dipole moments of layer V neocortical pyramidal cells
Row 1: cellular geometry of the three layer V pyramidal cells taken from Stuart & Spruston (1998). Row 2: intracellular potentials produced by current injection (200 pA) into the soma. Row 3: current dipole moment *Q* for the layer V pyramidal cells. Passive and active properties were taken from the 1996 Mainen model. Positive polarity indicates currents directed from a deep layer to the surface.

© 2006 The Authors. Journal compilation © 2006 The Physiological Society

the compartments. A positive volume vector moment corresponds to the direction pointing to pia. The mean and standard deviation were calculated for the four layer V pyramidal cells. The results supported the findings for Q. The volume vector moment was $-1457 \pm 1928\ \mu m^3$ for the basal segment and $9027 \pm 4874\ \mu m^3$ for the apical segment. The total volume vector element was larger for the apical than the basal segments consistent with the predominantly stronger apical spikes compared to the basal spikes. The mean and relatively large standard deviation for the basal segment are consistent with the existence of strong basal spikes that are predominantly directed away from the pia and the reversed polarity of the basal spike in one cell toward the pia. The statistics for

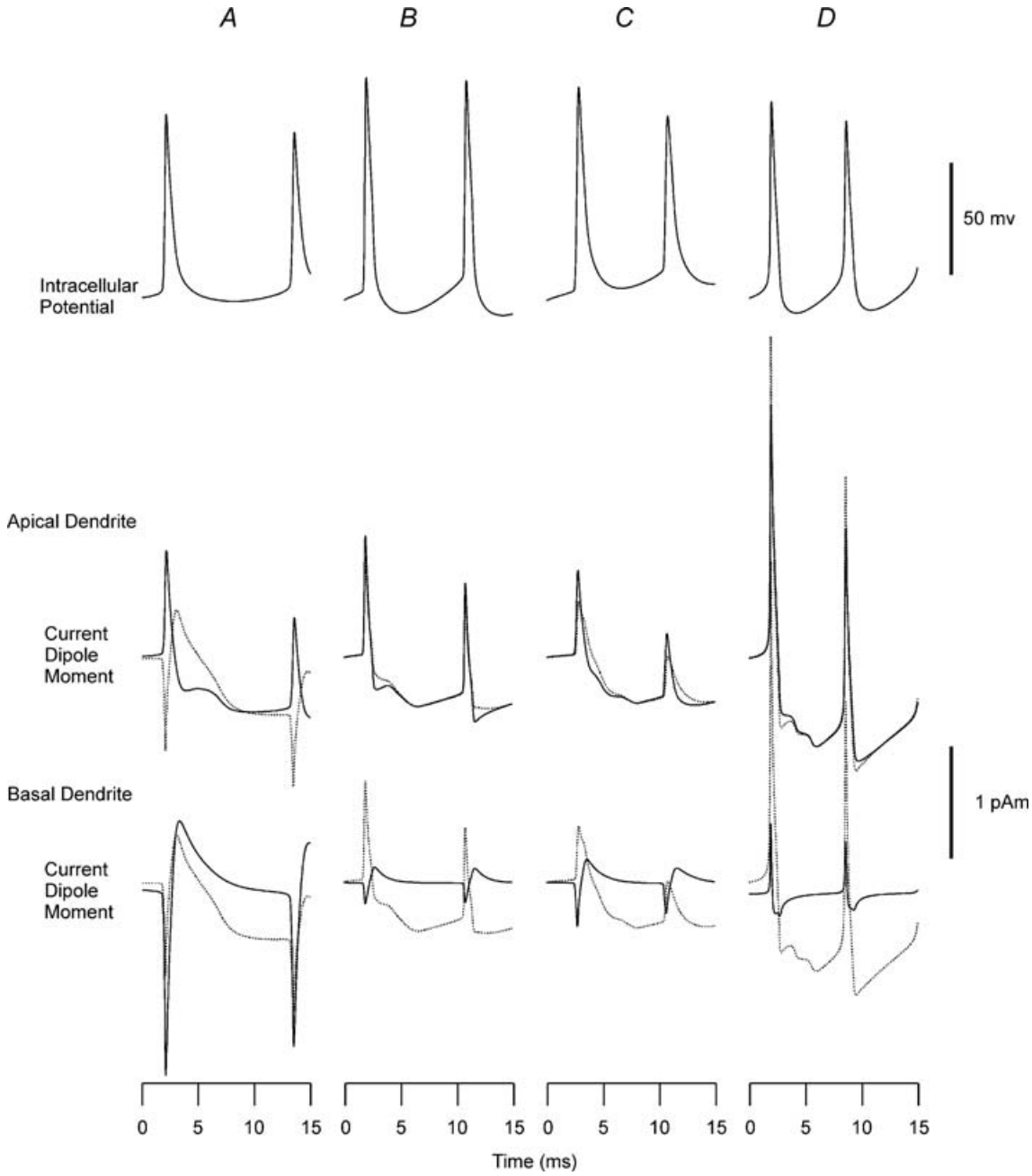

Figure 3. Contribution of dendrites to current dipole moments in layer V pyramidal cells
Row 1: intracellular potential from the four layer V pyramidal cells. Row 2: current dipole moment Q of a whole cell (dotted curve) and of the apical dendritic segments (continuous curves) for each cell. Row 3: current dipole moment Q of a whole cell (dotted curve) and of the basal dendritic segments (continuous curves) for each cell. *A*, layer V pyramidal cell from the 1996 Mainen model. *B–D*, three layer V pyramidal cells based on morphological data from Stuart & Spruston (1998).

© 2006 The Authors. Journal compilation © 2006 The Physiological Society

the apical segment indicate that the apical spikes should be strong and consistently directed toward the pia.

Contribution of sodium spikes to MEG and EEG

The next study investigated the dependence of the spikes on g_{Na} and $g_{K(DR)}$ distribution in the layer V pyramidal cell of the Mainen model (Fig. 4). First, effects of g_{Na} and $g_{K(DR)}$ on the spike were studied with these conductances present only in the soma and the axon, but not in the dendrites (Fig. 4*A*). This configuration corresponds to the classic concept of a CNS neuron with passive dendrites. The injection of inward current in the soma produced a simple sharp spike, which passively conducted to the adjacent basal and apical dendrites (Fig. 4*A* top). The intracellular potentials were delayed and less sharp at the basal terminal and at the first branch of the apical dendrite. The spike attenuated in amplitude with distance and did not reach the terminal of the apical dendrites. An attenuated spike could reach the terminal of the basal dendrites because of shorter electrical length. The *Q* for the whole cell was biphasic (Fig. 4*A* bottom). The initial spike component of *Q* was opposite in the apical and basal dendrites and tended to cancel each other, but the spike in the whole cell was predominantly due to the soma-basal dendrite segment in this Mainen model. The second spike component for a whole cell was predominantly due to the soma-basal segment because the terminals of the basal dendrites were depolarized due to their short electrical length. When a spike reaches the end of the dendrites, the potential gradient is directed toward the soma and thus current can flow from the dendritic terminal toward the soma. The spike in the soma-apical segment was nearly monophasic because the spike did not reach the terminal of the apical dendrites and the terminals were not depolarized. The spatial distribution of the current around a spike propagating in apical dendrites was nearly symmetrical and thus the waves on two sides of the spike tended to cancel each other.

In the second study, the active g_{Na} and $g_{K(DR)}$ were introduced into the apical and basal dendrites to model a CNS neuron consistent with recent findings (Fig. 4*B–D*). As mentioned in Methods, the densities were adjusted in order for the model neuron to be capable of producing the backpropagation of action potentials into the apical dendrites and basal dendrites (Stuart & Sakmann, 1994; Larkum *et al.* 1999; Williams & Stuart, 2000; Antic, 2003). In Fig. 4*B*, the active g_{Na} and $g_{K(DR)}$ were extended to the basal and proximal apical dendrites, but not to the distal apical dendrites to simulate the back-propagation failing to invade the distal apical dendrites. The somatic current injection produced a sharp spike initially in the soma (Fig. 4*B* top). The spike then propagated toward the terminals of the apical dendrites with amplitude

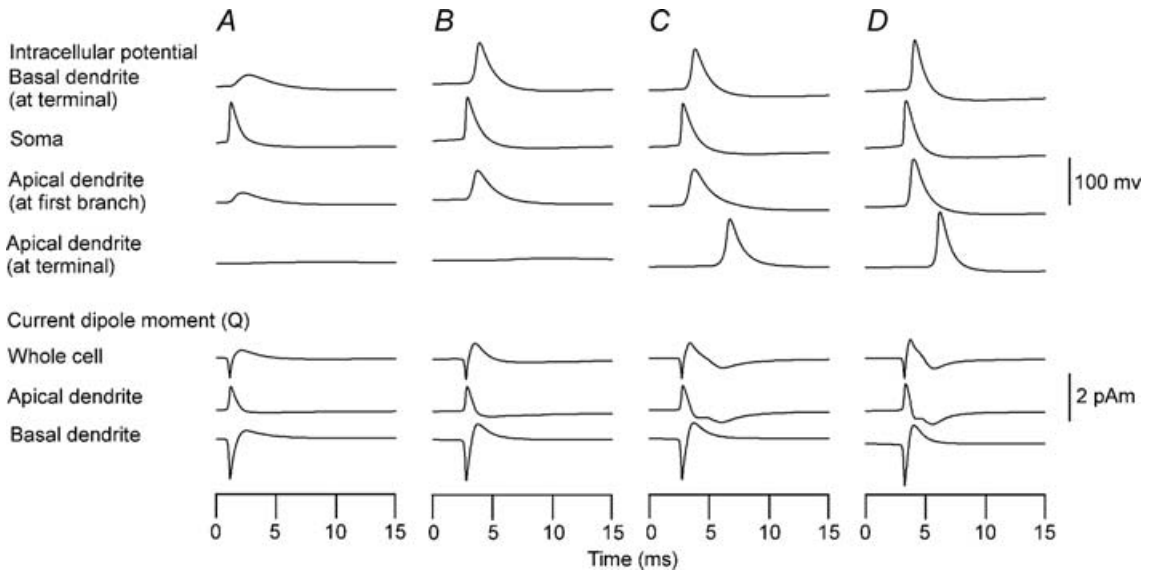

Figure 4. Contribution of sodium conductance g_{Na} and potassium conductance of delayed rectifier $g_{K(DR)}$ in a layer V pyramidal neuron with varying active channel properties
Top four rows: intracellular potentials at basal dendritic terminal (row 1), soma (row 2), first branching point of the apical dendrite (row 3), and apical dendritic terminal (row 4). Bottom three rows: current dipole moments of whole cell (row 5), apical dendritic segment (row 6) and basal dendritic segment (row 7). *A*, cell with g_{Na} and $g_{K(DR)}$ only in the soma with passive basal and apical dendrites. *B*, cell with g_{Na} and $g_{K(DR)}$ distributed throughout the basal and proximal apical dendrites up to the first branching point. *C*, same as cell in b except g_{Na} and $g_{K(DR)}$ were distributed uniformly throughout the dendrites. $g_{Na} = 40$ pS μm^{-2} for cells in *A–C*. *D*, same as cell in c except $g_{Na} = 100$ pS μm^{-2}.

© 2006 The Authors. Journal compilation © 2006 The Physiological Society

attenuation and could not reach the terminals of the apical dendrites. The spike reached the terminal of basal dendrites because all of the basal dendrites were active. The Q of the whole cell was biphasic as in the classic neuron model (Fig. 4*B* bottom). However, the second phase of the Q became larger because of the contribution of active basal dendrites. The biphasic spike wave in the soma-basal segment was similar to the waveform of the classic neuron with passive dendrites, but the wave was faster and stronger than the classic neuron. This is due to the larger spike that arrived at the terminal of the basal dendrites earlier than the classic neuron. When the active g_{Na} and $g_{K(DR)}$ were extended to the distal apical dendrites (Fig. 4*C*), the somatic current injection produced a sharp spike in the soma as in Fig. 4*A* and *B*. However, the spike then propagated toward the terminals of both the apical and basal dendrites without any amplitude attenuation or significant widening of the spike width (Fig. 4*C* top). In this model with uniformly active dendrites, the Q changed from the biphasic waveform of Fig. 4*A* and *B* to a triphasic waveform (Fig. 4*C* bottom). The Q of the whole cell consisted of a spike wave complex followed by a slower deflection. The Q for the soma-apical segment was considerably different from the first two models. The wave portion following the spike was stronger and more complex in shape than the first two neurons because the spike propagated as far as the terminal of the apical dendrites. By comparing the waveforms for the whole cell and the two dendritic segments of the neuron, it can be seen that the initial spike wave was due to the biphasic wave produced in the basal segment and the next slow component was due to the spike propagating toward the apical terminal. Thus, the duration of Na^+ spike wave complex lasting several milliseconds is dependent on the duration of Na^+ spike propagation within the apical dendrites.

In the next simulation, the stability of the spike wave complex was tested for another channel density of g_{Na} (Fig. 4*D*). The channel density was increased from 40 pS μm^{-2} to 100 pS μm^{-2}. The magnitude of spikes in intracellular potential became slightly larger, but their behaviour did not change in general because of the stability of the Hodgkin-Huxley-type equation (Fig. 4*D* top). Similarly, the Q did not significantly change in amplitude and shape, although the duration is generally shorter for this model with a higher channel density than the previous model (Fig. 4*D* bottom). Our results for the spikes were thus relatively invariant with regard to g_{Na} over the range of 40–100 pS μm^{-2}.

Discussion

This study provided a quantitative estimate of the Q for a realistically shaped cell for each of the four principal neuron classes. The layer V and layer II/III pyramidal cells with an open-field configuration were capable of producing stronger Q, whereas the layer IV spiny stellate and layer III aspiny stellate cell with closed-field configurations produced weaker Qs. The overall magnitude was generally in agreement with the concept of open- and closed-field configuration of neurons proposed by Lorente de Nó (1947).

The overall magnitude of $\boldsymbol{Q}$ for the pyramidal cells was much stronger than some earlier calculations, but agrees with other previous, independently obtained empirical and theoretical estimates. The magnitude in this study was 0.29–0.90 pA m for the envelopes of the layer V and layer II/III pyramidal cells. This is 15–45 times stronger than the estimate of 0.02 pA m calculated by Hämäläinen *et al.* (1993). They computed the Q for a classic cell with passive cylindrical dendrites, assuming dendritic diameter of 1 μm, intracellular conductivity of 1 S m^{-1}, and a postsynaptic potential of 25 mV, which was incidentally very large and could shift the intracellular potential from a resting level to a value above the Na^+ spike threshold. The values of Q obtained in the present simulation study, however, agree with the empirical estimates obtained for hippocampal pyramidal cells. The Q was estimated to be 0.2 pA m $cell^{-1}$ for the CA1 pyramidal cells and 0.17 pA m $cell^{-1}$ for CA3 pyramidal cells (Kyuhou & Okada, 1993; Okada *et al.* 1997). These values are virtually the same as 0.29 pA m $cell^{-1}$ found for the envelope of Q for the layer II/III pyramidal cell and within a factor of about 2 (0.41–0.90 pA m $cell^{-1}$) for the envelope of the layer V pyramidal cells. These values are also quite similar to the theoretical values for the envelope of Q found for the CA3 slice model (Murakami *et al.* 2002, 2003). The initial spike and the subsequent envelope were +0.21 and −0.25 pA m, respectively, for the CA3 cell, whereas they were +0.45 and −0.27 pA m, respectively, for the layer II/III pyramidal cell (Zhang *et al.* unpublished observations). The Qs of measurable cortical generators in humans are generally on the order of 10 nA m (Hämäläinen *et al.* 1993). Assuming a Q of 0.2 pA m $cell^{-1}$ for cortical pyramidal neurons, an ensemble of 50 000 synchronously firing neurons may be sufficient to generate such signals. Since the passive and active membrane properties are similar across mammals (Hille, 2001), our results suggest that MEG and EEG may be sufficiently sensitive to detect cortical activity occurring even within a small number of cortical columns in the human brain.

In addition to providing quantitative estimates of the Q that may be produced by the principal neurons, the present analysis revealed some results that were counter-intuitive in some respects. First, neocortical model neurons were found to be capable of producing sodium spikes with dipolar moments in whole cells that were considerably strong (−0.78 to 2.97 pA m). Assuming a rough value of 1 pA m for the dipole moment of a spike/cell, an ensemble

© 2006 The Authors. Journal compilation © 2006 The Physiological Society

of 10 000 synchronized neurons may produce a population Q of approximately 10 nA m. It has been assumed that sodium spikes do not contribute to MEG and EEG signals because the spikes produced by a population of pyramidal cells tend to cancel each other due to temporal jitter (De Munck *et al.* 1992). However, recent studies indicate that the brain of many species is capable of producing spikes with an extremely high degree of synchronization having a temporal jitter of less than a millisecond (Jones *et al.* 2000; Barth, 2003; Kato *et al.* 2003). The temporal jitter is apparently sufficiently small for the detection of high-frequency cortical signals (Curio *et al.* 1994; Hashimoto *et al.* 1996; Ikeda *et al.* 2002, 2005). Thus, the Qs for the sodium spikes may summate across a population of pyramidal neurons with little loss of signal and produce detectable signals. The relative strengths of population spikes and slower waves, however, obviously depend on the degree of synchronization of the neurons. The spikes may be relatively strong when the neurons are completely synchronized as in the case considered here. In the model studies of CA3 by Murakami *et al.* (2002, 2003), the spikes as well as slower waves could be seen in the population Q for the pyramidal neurons simultaneously stimulated by an extracellualr stimulus. Strong sodium spikes can be seen empirically in CA3 slices (Zhang *et al.* unpublished observations). The population Q due to synaptically activated neurons, however, was completely due to their slow waves. An examination of the Qs produced by the individual neurons in this case showed that the Q contained a spike train riding on a current of depolarization shift just as in the neocortical neurons (Zhang *et al.* unpublished observations).

The simulation results also showed that the basal dendrites may be capable of producing sodium spikes. It has been believed that basal dendrites do not make a significant contribution to MEG and EEG signals because of their short diameters and symmetric structure (Hämäläinen *et al.* 1993). However, the present results showed that basal dendrites could contribute to MEG and EEG signals. A statistical analysis of the primary dendrites of pyramidal cells has demonstrated that the primary basal dendrites have a preference for extending toward a deep layer (Staiger *et al.* 2004). The volume vector element analysis in the present study corroborates this conclusion. The same tendency is commonly found in much of the literature (Kawaguchi, 1993; Thomson *et al.* 1996; Larkum *et al.* 1999, 2001; Antic, 2003).

Another unexpected result was the magnitude of dipolar current produced by two stellate cells. The peak-to-baseline spike amplitudes were 0.27 pA m for a spiny stellate cell and 0.06 pA m for an aspiny stellate cell. The amplitude for the spiny stellate cell is of the same order of magnitude as the spikes produces by the pyramidal cells. Although unexpected, the result for the spiny stellate cell is consistent with the statistical result of Staiger *et al.* (2004). These investigators found that the primary dendrites of spiny stellate cells in the neocortex abundantly originate at 90–180 deg away from the axis directed toward the pia. The strong dipole moment is also consistent with the volume vector element analysis for the spiny stellate cell in this study. The net vector moment was $-865\ \mu m^3$, pointing toward a deeper layer.

Nevertheless, the Q for a population of stellate cells may be much weaker than the values based on a linear summation of Qs for individual neurons. The $\boldsymbol{Q}$ calculated for the spiny stellate cell was oriented along the direction of strongest net moment for the cell. However, the orientation of the net $\boldsymbol{Q}$ is variable for the dendrites of the spiny stellate cells as well as aspiny stellate cells. Thus, the population Q may be diminished by this variability in dendritic geometry.

These results contrary to some classic assumptions indicate that quantitative examination is indeed necessary to carefully investigate the origins of MEG and EEG signals. This conclusion is quite important today since the anatomical data on the three-dimensional structure of cortical neurons are beginning to become available and electrophysiological data are available for constructing realistic mathematical models of cortical neurons. In the present study the neocortical model neurons lacked extended axonal arbors due to lack of available anatomical data. However, this structure may need to be included in evaluating the sodium spikes. If the axons are aligned parallel to each other in a population of cells, these axonal spikes could summate and possibly be detectable outside the brain. Moreover some types of neocortical cells have an asymmetric spatial arrangement for axons (Karube *et al.* 2004). In such a case the axons might generate a significant population signal. The present results are also relevant for examining MEG and EEG signals from structures other than the neocortex and hippocampus. The open/closed field theory is usually applied to these structures in which the contrast between cell shapes of open field type (e.g. pyramidal cells and Purkinje cells) and closed field type (e.g. interneurons) is relatively clear. However, MEG and EEG signals are also measured from various areas of the central nervous system, including the cerebellum and the subcortical region such as the thalamus in which the contrast is not clear. A mathematical model of realistically shaped neurons may be useful for these structures.

The waveform of Q reflects properties of active channels in the neurons. The pyramidal cells capable of bursting (Connors & Gutnick, 1990) produced a Q consisting of a train of sharp spike waves riding on an envelope shape in Q. The spikes and envelope corresponded to the spike train and depolarization shift seen in intracellular potential. The Q of both the spiny and aspiny stellate cells consisted of a train of spike waves without the envelope, corresponding to the tonic firing without a burst in intracellular potential. The contributions of

© 2006 The Authors. Journal compilation © 2006 The Physiological Society

active ionic conductances to the envelope of Q were analysed in some detail by Murakami *et al.* (2002, 2003). In their comparisons of theoretical and empirical MEG data for the CA3 slice preparation, they found that g_{Ca} and g_{KCa} play crucial roles in shaping the envelope reflecting the depolarization shift and subsequent slower waves. In the present study the generation of spikes were analysed in some detail since the spikes from individual cortical neurons were found to be unexpectedly strong. The analysis demonstrated that the spike is relatively stable in amplitude and waveform for a range of g_{Na} conductance varying by a factor of 2.5. The subsequent portion of the complex, however, depends on the active properties of the dendrites. The g_{Na} and $g_{K(DR)}$ present in the distal apical dendrites produced spike propagation into the terminals, which resulted in the prolonged Q. These simulation studies of the spike-complex corroborate our general claim that it is necessary to understand the behaviour of neocortical neurons using realistic models of the cells incorporating active conductances in order to obtain fundamental insights into the genesis of MEG and EEG signals.

References

Antic SD (2003). Action potentials in basal and oblique dendrites of rat neocortical pyramidal neurons. *J Physiol* **550**, 35–50.

Barr RC, Pilkington TC, Boineau JP & Spach MS (1966). Determining surface potentials from current dipoles, with application to electrocardiography. *IEEE Trans Biomed Eng* **13**, 88–92.

Barth DS (2003). Submillisecond synchronization of fast electrical oscillations in neocortex. *J Neurosci* **23**, 2502–2510.

Bekkers JM (2000). Properties of voltage-gated potassium currents in nucleated patches from large layer 5 cortical pyramidal neurons of the rat. *J Physiol* **525**, 593–609.

Connors BW & Gutnick MJ (1990). Intrinsic firing patterns of diverse neocortical neurons. *Trends Neurosci* **13**, 99–104.

Curio G, Mackert BM, Burghoff M, Koetitz R, Abraham-Fuchs K & Harer W (1994). Localization of evoked neuromagnetic 600 Hz activity in the cerebral somatosensory system. *Electroencephalogr Clin Neurophysiol* **91**, 483–487.

De Munck JC, Vijn PC & Lopes da Silva FH (1992). A random dipole model for spontaneous brain activity. *IEEE Biomag Eng* **39**, 791–804.

Geselowitz DB (1967). On bioelectric potentials in an inhomogeneous volume conductor. *Biophys J* **7**, 1–11.

Geselowitz DB (1970). On the magnetic field generated outside an inhomogeneous volume conductor by internal current sources. *IEEE Trans Mag* **6**, 346–347.

Hämäläinen M, Hari R, Ilmoniemi R, Knuutila J & Lounasmaa O (1993). Magnetoencephalography. Theory, instrumentation and applications to the noninvasive study of human brain function. *Rev Mod Phys* **65**, 413–497.

Hashimoto I, Mashiko T & Imada T (1996). High-frequency magnetic signals in the human somatosensory cortex. *Electroencephalogr Clin Neurophysiol Suppl* **47**, 67–80.

Haydon PG (2001). GLIA: listening and talking to the synapse. *Nature Rev Neuroscience* **2**, 185–193.

Hille B (2001). *Ionic Channels of Excitable Membranes*. Sinauer, Sunderland, MA, USA.

Huang JC, Nicholson C & Okada YC (1990). Distortion of magnetic evoked fields and surface potentials by conductivity differences at boundaries in brain tissue. *Biophys J* **57**, 1155–1166.

Huguenard JR, Hamill OP & Prince DA (1988). Developmental changes in Na^+ conductances in rat neocortical neurons: appearance of a slowly inactivating component. *J Neurophysiol* **59**, 778–795.

Ikeda H, Leyba L, Bartolo A, Wang Y & Okada YC (2002). Synchronized spikes of thalamocortical axonal terminals and cortical neurons are detectable outside the pig brain with MEG. *J Neurophysiol* **87**, 626–630.

Ikeda H, Wang Y & Okada YC (2005). Origins of the somatic N20 and high-frequency oscillations evoked by trigeminal stimulation in the piglets. *Clin Neurophysiol* **116**, 827–841.

Johnston D, Magee JC, Colbert CM & Cristie BR (1996). Active properties of neuronal dendrites. *Annu Rev Neurosci* **19**, 165–186.

Jones MS, MacDonald KD, Choi B, Dudek FE & Barth DS (2000). Intracellular correlates of fast (>200 Hz) electrical oscillations in rat somatosensory cortex. *J Neurophysiol* **84**, 1505–1518.

Karube F, Kubota Y & Kawaguchi Y (2004). Axon branching and synaptic bouton phenotypes in GABAergic nonpyramidal cell subtypes. *J Neurosci* **24**, 2853–2865.

Kato S, Wang Y, Papuashvili N & Okada YC (2003). Stable synchronized high-frequency signals from the main sensory and spinal nuclei of the pig activated by Aβ fibers of the maxillary nerve innervating the snout. *Brain Res* **959**, 1–10.

Kawaguchi Y (1993). Grouping of nonpyramidal and pyramidal cells with specific physiological and morphological characteristics in rat frontal cortex. *J Neurophysiol* **69**, 416–431.

Korngreen A & Sakmann B (2000). Voltage-gated K^+ channels in layer 5 neocortical pyramidal neurones from young rats: subtypes and gradients. *J Physiol* **525**, 621–639.

Kyuhou S & Okada YC (1993). Detection of magnetic signals from isolated transverse CA1 hippocampal slice of the guinea pig. *J Neurophysiol* **70**, 2665–2668.

Larkum ME, Kaiser KM & Sakmann B (1999). Calcium electrogenesis in distal apical dendrites of layer 5 pyramidal cells at a critical frequency of back-propagating action potentials. *Proc Natl Acad Sci U S A* **96**, 14600–14604.

Larkum ME, Zhu JJ & Sakmann B (2001). Dendritic mechanisms underlying the coupling of the dendritic with the axonal action potential initiation zone of adult rat layer 5 pyramidal neurons. *J Physiol* **533**, 447–466.

Llinás RR (1988). The intrinsic electrophysiological properties of mammalian neurons: Insights into central nervous system function. *Science* **242**, 1654–1664.

© 2006 The Authors. Journal compilation © 2006 The Physiological Society

Llinás RR & Nicholson C (1974). Analysis of field potential in the central nervous system. *Handbook Electroenceph Clin Neurophysio* **2B**, 61–83.

Lorente de No R (1947). Action potential of the motoneurons of the hypoglossus nucleus. *J Cell Comp Physiol* **29**, 207–287.

Mainen ZF & Sejnowski TJ (1996). Influence of dendritic structure on firing pattern in model neocortical neurons. *Nature* **382**, 363–366.

Migliore M & Shepherd GM (2002). Emerging rules for the distributions of active conductances. *Nat Rev Neurosci* **3**, 362–370.

Murakami S, Hirose A & Okada YC (2003). Contribution of ionic currents to magnetoencephalography (MEG) and electroencephalography (EEG) signals generated by guinea-pig CA3 slices. *J Physiol* **553**, 975–985.

Murakami S, Zhang T, Hirose A & Okada YC (2002). Physiological origins of evoked magnetic fields and extracellular field potentials produced by the guinea-pig CA3. *J Physiol* **544**, 237–251.

Okada YC (1982). Neurogenesis of evoked magnetic fields. In *Biomagnetism an Interdisciplinary Approach*, ed. Williamson SJ, Romani GL, Kaufman L & Modena L, pp. 399–408. Plenum Press, New York and London.

Okada YC & Wu J (1998). Interpretation of evoked magnetic fields, evoked field potentials and intracellular potentials of the longitudinal CA3 slice within a modern theoretical framework. *Soc Neurosci Abstr* **24**, 1180.

Okada YC, Wu J & Kyuhou S (1997). Genesis of MEG signals in a mammalian CNS structure. *Electroenceph Clin Neurophysiol* **103**, 474–485.

Sarvas J (1987). Basic mathematical and electromagnetic concepts of the biomagnetic inverse problem. *Phys Med Biol* **32**, 11–22.

Schiller J, Helmechen F & Sakmann B (1995). Spatial profile of dendriric transient evoked by action potential in rat neocortical pyramidal neurones. *J Physiol* **487**, 583–600.

Staiger JF, Flagmeyer I, Schubert D, Zilles K, Kotter R & Luhmann HJ (2004). Functional diversity of layer IV spiny neurons in rat somatosensory cortex: quantitative morphology of electrophysiologically characterized and biocytin labeled cells. *Cereb Cortex* **14**, 690–701.

Stuart GJ & Sakmann B (1994). Active propagation of somatic action potentials into neocortical pyramidal cell dendrites. *Nature* **367**, 69–72.

Stuart GJ & Spruston N (1998). Determinants of voltage attenuation in neocortical pyramidal neuron dendrtes. *J Neurosci* **18**, 3501–3510.

Thomson AM, West DC, Hahn J & Deuchars J (1996). Single axon IPSPs elicited pyramidal cells by three classes of interneurons in slices of rat ceocortex. *J Physiol* **496**, 81–102.

Traub RD, Jefferys JGR & Miles R (1993). Analysis of the propagation of disinhibition-induced after-discharged along the guinea-pig hippocampal slice *in vitro*. *J Physiol* **472**, 267–287.

Traub RD, Jefferys JGR, Miles R, Whittington MA & Tóth K (1994). A branching dendritic model of a rodent CA3 pyramidal neurone. *J Physiol* **481**, 79–95.

Traub RD, Jefferys JGR & Whittington MA (1999). *Fast Oscillations in Cortical Circuits*. MIT Press, Cambridge, MA, USA.

Traub RD & Miles R (1991). *Neuronal Networks of the Hippocampus*. Cambridge University Press, New York.

Traub RD, Miles R & Buzsaki G (1992). Computer simulation of carbachol-driven rhythmic population oscillations in the CA3 region of the *in vitro* rat hippocampus. *J Physiol* **451**, 653–672.

Traub RD, Wong RKS, Miles R & Michelson H (1991). A model of a CA3 hippocampal pyramidal neuron incorporating voltage-clamp data on intrinsic conductances. *J Neurophysiol* **66**, 635–650.

Williams SR & Stuart GJ (2000). Backpropagation of physiological spike trains in neocortical pyramidal neurons: implications for temporal coding in dendrites. *J Neurosci* **20**, 8238–8246.

Acknowledgements

This work was supported financially by the NIH grants R03-NS50544 to S, Murakami and R01-NS21149 to Y. Okada. We thank J. Nurminen, A. O'Meara, H. Ishibashi and S. Mun-Bryce for comments about the manuscript.

© 2006 The Authors. Journal compilation © 2006 The Physiological Society